View metadata, citation and similar papers at core.ac.uk

brought to you by CORE

provided by NASA Technical Reports Server

NASA/TM—1999-209080

AIAA–99–0745

Implementation and Validation of the Chien k-ϵ Turbulence Model in the Wind Navier-Stokes Code

Dennis A. Yoder and Nicholas J. Georgiadis
Glenn Research Center, Cleveland, Ohio

Prepared for the
37th Aerospace Sciences Meeting & Exhibit
sponsored by the American Institute of Aeronautics and Astronautics
Reno, Nevada, January 11–14, 1999

National Aeronautics and
Space Administration

Glenn Research Center

April 1999

Trade names or manufacturers' names are used in this report for identification only. This usage does not constitute an official endorsement, either expressed or implied, by the National Aeronautics and Space Administration.

Available from

NASA Center for Aerospace Information
7121 Standard Drive
Hanover, MD 21076
Price Code: A03

National Technical Information Service
5285 Port Royal Road
Springfield, VA 22100
Price Code: A03

IMPLEMENTATION AND VALIDATION OF THE CHIEN k-ϵ TURBULENCE MODEL IN THE WIND NAVIER-STOKES CODE

Dennis A. Yoder *
Nicholas J. Georgiadis †
National Aeronautics and Space Administration
Glenn Research Center
Cleveland, Ohio

Abstract

The two-equation $k-\epsilon$ turbulence model of Chien has been implemented in the WIND Navier-Stokes flow solver. Details of the numerical solution algorithm, initialization procedure, and stability enhancements are described. Results obtained with this version of the model are compared with those from the Chien $k-\epsilon$ model in the NPARC Navier-Stokes code and from the WIND SST model for three validation cases: the incompressible flow over a smooth flat plate, the incompressible flow over a backward facing step, and the shock-induced flow separation inside a transonic diffuser. The $k-\epsilon$ model results indicate that the WIND model functions very similarly to that in NPARC, though the WIND code appears to be slightly more accurate in the treatment of the near-wall region. Comparisons of the $k-\epsilon$ model results with those from the SST model were less definitive, as each model exhibited strengths and weaknesses for each particular case.

Nomenclature

a	speed of sound
C_f	local skin friction coefficient
E	total energy per unit volume
H	step height, diffuser height
H^*	diffuser throat height
i, j, k	computational coordinate indices
k, k^+	turbulent kinetic energy, $k^+ = k/u_\tau^2$
M_t	turbulent Mach number
P, P_t	static, total pressure
P_o	plenum pressure
Re	Reynolds number based on reference conditions, $a_\infty L/\nu_\infty$
Re_t	Reynolds number based on turbulence quantities
Re_x	Reynolds number based on axial position
T, T_t	static, total temperature
t	time
U, V, W	contravarient velocity components
u, v, w	Cartesian velocity components
$u_{ref(k-\epsilon)}$	reference velocity for turbulent kinetic energy limiter
u_τ	friction velocity, $\sqrt{\tau_w/\rho}$
u^+	normalized velocity, u/u_τ
$-\overline{uv}, -\overline{uv}^+$	Reynolds stress, $-\overline{uv}^+ = -\overline{uv}/u_\tau^2$
x, y, z	Cartesian coordinates
x_r	reattachment location
y^+	normalized distance from wall, yu_τ/ν
ϵ, ϵ^+	rate of dissipation of turbulent kinetic energy, $\epsilon^+ = \nu\epsilon/u_\tau^4$
γ	ratio of specific heats
μ, μ_t	laminar, turbulent viscosity
ν	laminar kinematic viscosity, μ/ρ
Π	production of turbulent kinetic energy
ρ	density
$\sigma_k, \sigma_\epsilon$	turbulent Prandtl numbers
ξ, η, ζ	curvilinear coordinates

Difference Operators

$$\begin{aligned}
\triangle_\xi Q_{i,j,k} &= (Q_{i+1,j,k} - Q_{i,j,k})/\triangle\xi \\
\nabla_\xi Q_{i,j,k} &= (Q_{i,j,k} - Q_{i-1,j,k})/\triangle\xi \\
\overline{\delta}_\xi Q_{i,j,k} &= (Q_{i+1,j,k} - Q_{i-1,j,k})/2\triangle\xi \\
\delta_\xi Q_{i,j,k} &= (Q_{i+\frac{1}{2},j,k} - Q_{i-\frac{1}{2},j,k})/\triangle\xi \\
\mu_\xi Q_{i,j,k} &= (Q_{i+\frac{1}{2},j,k} + Q_{i-\frac{1}{2},j,k})/2
\end{aligned}$$

Introduction

In 1992, NASA Lewis Research Center (LeRC) and Arnold Engineering Development Center (AEDC) formed a partnership to enhance the military and commercial competitiveness of the Unites States through the establishment of the NPARC computational fluid dynamics code. This NPARC Alliance has developed and supported the code by drawing from the talents of individuals at both centers as well as from other organizations outside the Alliance.

*AIAA Member
†AIAA Senior Member

Copyright © 1999 by the American Institute of Aeronautics and Astronautics, Inc. No copyright is asserted in the United States under Title 17, U.S. Code. The U.S. Government has a royalty-free license to exercise all rights under the copyright claimed herein for Governmental Purposes. All other rights are reserved by the copyright owner.

As explained in reference 1, recent events have led the Alliance to undertake the formidable task of combining the predictive capabilities of three Navier-Stokes flow solvers into a new code called WIND. These solvers are the NPARC code of the NPARC Alliance, the NASTD code from the McDonnell Douglas Corporation which is now part of the Boeing Company, and the NXAIR code. The NASTD code was selected as the foundation for the new WIND code, primarily because it offered the most features of the three codes. Much of the Alliance's work for the past two years has focused on incorporating the desirable features of the other two codes into the NASTD framework.

At the time of the merger, the NASTD code offered a variety of turbulence modeling options including the algebraic models of P.D. Thomas, Cebeci-Smith, and Baldwin-Lomax, the one-equation models of Baldwin-Barth and Spalart-Allmaras, and the two-equation Shear-Stress Transport (SST) model of Menter[2]. A variety of $k-\epsilon$ models had also been incorporated into the code, but were only moderately stable and required the user to be well-versed in the art of turbulence modeling. These $k-\epsilon$ models were subsequently removed from the code prior to the merger activity.

Meanwhile, users of the NPARC code have had success with the Chien[3] $k-\epsilon$ model. The NPARC implementation has proven to be relatively robust and numerically stable for many types of flows. Of the low Reynolds number $k-\epsilon$ models evaluated by Patel, Rodi, and Scheuerer[4], the models of Chien, Launder-Sharma, and Lam-Bremhorst were found to perform the best and yielded comparable results. For adverse pressure gradient flows, Wilcox[5] showed the Chien and Launder-Sharma models to be the best of the $k-\epsilon$ models. For these reasons it was decided to include the NPARC Chien $k-\epsilon$ model into the WIND code.

The purpose of this report is threefold: (1) Combine all of the modifications of previous developers into a single complete and concise reference, (2) Present several validation cases for the present implementation, (3) Compare results from the Chien $k-\epsilon$ models in the NPARC and WIND flow solvers with those from the SST model in the WIND code.

This will hopefully aid users of the NPARC code in transitioning to WIND by providing a direct code to code comparison of the results obtained using the same computational mesh and turbulence model. In addition, results from the WIND SST model will also be included to demonstrate some of the strengths and weaknesses of each model.

Numerical Algorithm

Development of the Chien k-ϵ model in the NPARC flow solver has been aided by several authors over the years. The basic algorithm for solving the turbulent transport equations is described by Nichols[6] with some stability enhancements added by Georgiadis, Chitsomboon, and Zhu[7].

For the WIND implementation, the $k-\epsilon$ equations are nondimensionalized in a manner consistent with the mean-flow equations in the following way:

$$\begin{aligned} x &= x'/L' & P &= P'/\gamma P'_\infty \\ \rho &= \rho'/\rho'_\infty & T &= T'/T'_\infty \\ u &= u'/a'_\infty & E &= E'/\rho'_\infty a'^2_\infty \\ \mu &= \mu'/\mu'_\infty & k &= k'/a'^2_\infty \\ \mu_t &= \mu'_t/\mu'_\infty & \epsilon &= \epsilon'/\left(a'^3_\infty/L'\right) \end{aligned}$$

Transforming to generalized curvilinear coordinates, the $k-\epsilon$ equations can be written as

$$\frac{\partial Q}{\partial \tau} + \frac{\partial F_i}{\partial \xi_i} = \frac{\partial G_i}{\partial \xi_i} + S$$

$$Q = J^{-1}\begin{bmatrix} \rho k \\ \rho \epsilon \end{bmatrix}$$

$$F_i = J^{-1}\begin{bmatrix} \rho U_i k \\ \rho U_i \epsilon \end{bmatrix}$$

$$G_i = (J\,Re)^{-1}\begin{bmatrix} \mu_k \nabla \xi_i \cdot \nabla k \\ \mu_\epsilon \nabla \xi_i \cdot \nabla \epsilon \end{bmatrix}$$

$$S = (J\,Re)^{-1}\begin{bmatrix} \Pi - \rho\epsilon\,(1 + F(M_t))\,Re - 2\mu\frac{k}{y^2} \\ C_{\epsilon 1} f_1 \Pi \frac{\epsilon}{k} - C_{\epsilon 2} f_2 \frac{\rho \epsilon^2}{k} Re - 2\mu \frac{\epsilon}{y^2}\epsilon^{(-y^+/2)} \end{bmatrix}$$

$$\Pi = \mu_t \frac{\partial u_i}{\partial x_j}\left[\frac{\partial u_i}{\partial x_j} + \frac{\partial u_j}{\partial x_i}\right] - \frac{2}{3}\frac{\partial u_i}{\partial x_j}\left(\mu_t \frac{\partial u_k}{\partial x_k} + \rho k\right)\delta_{ij} Re$$

$$\begin{aligned} \mu_k &= \mu + \mu_t/\sigma_k \\ \mu_\epsilon &= \mu + \mu_t/\sigma_\epsilon \\ \mu_t &= C_\mu f_\mu \frac{\rho k^2}{\epsilon} Re \\ Re_t &= \frac{\rho k^2}{\mu \epsilon} Re \\ f_1 &= 1.0 \\ f_2 &= 1.0 - 0.22 \exp\left(-(Re_t/6)^2\right) \\ f_\mu &= 1.0 - \exp\left(-0.0115 y^+\right) \end{aligned}$$

where $C_\mu = 0.09$, $C_{\epsilon 1} = 1.35$, $C_{\epsilon 2} = 1.80$, $\sigma_k = 1.0$, $\sigma_\epsilon = 1.3$.

Early results with the $k-\epsilon$ model in the NPARC code revealed that nonphysical negative production terms could arise through the use of the complete production term. Thus, terms on the second line of the II definition are neglected, which corresponds to use of the incompressible form. This same approach has been used in the WIND code.

To enhance predictions at higher Mach numbers, a compressibility correction of the form

$$F(M_t) = \alpha_k \cdot Max\left(M_t^2 - M_{t_0}^2, 0\right)$$

has been added, and selection of the Sarkar[8] or Wilcox[9] compressibility corrections is done through the specification of the constants α_k and M_{t_0} as indicated in Table 1. The turbulent Mach number used in these corrections is defined as $M_t^2 = 2k/a^2$, where a is the local speed of sound. Note that the compressibility correction can be turned off by setting α_k to 0.

Table 1: Constants used in selecting the compressibility correction.

α_k	M_{t0}	Correction Type
1.0	0.00	Sarkar
1.5	0.25	Wilcox
0.0	0.00	None

Both the Sarkar and Wilcox compressibility corrections are designed to improve the prediction of compressible flow jets by including the compressible portion of the dissipation rate in the transport equation for the turbulent kinetic energy. These corrections use simple algebraic relations between the solenoidal and compressible dissipation rates. The effect of these corrections is to reduce the turbulent kinetic energy in compressible flow regions. In terms of supersonic jet predictions, this results in slower jet spreading rates, reduced mixing, and a longer core length.

The turbulent transport equations described above are solved decoupled from the main flow solver using an approximate factorization approach

$$\widehat{RHS} = \Delta\tau\,(\,-\partial_\xi F_1^n - \partial_\eta F_2^n - \partial_\zeta F_3^n + \partial_\xi G_1^n + \partial_\eta G_2^n + \partial_\zeta G_3^n + \hat{S}^n\,)$$

$$\begin{aligned}
\left[I + \Delta\tau\left(\nabla_\xi \hat{A}_1^+ + \Delta_\xi \hat{A}_1^- - \delta_\xi \hat{B}_1\right)\right]\Delta\hat{Q}^{**} &= \widehat{RHS} \\
\left[I + \Delta\tau\left(\nabla_\eta \hat{A}_2^+ + \Delta_\eta \hat{A}_2^- - \delta_\eta \hat{B}_2 - \hat{C}\right)\right]\Delta\hat{Q}^{*} &= \Delta\hat{Q}^{**} \\
\left[I + \Delta\tau\left(\nabla_\eta \hat{A}_3^+ + \Delta_\zeta \hat{A}_3^- - \delta_\zeta \hat{B}_3\right)\right]\Delta\hat{Q} &= \Delta\hat{Q}^{*}
\end{aligned}$$

where the operators $\nabla_\xi, \Delta_\xi, \delta_\xi$ operate through ΔQ^{**}. A, B, and C are the Jacobian matrices resulting from the linearization of F, G, and S.

$$\begin{aligned}
A_i^\pm &= \begin{bmatrix} U_i^\pm & 0 \\ 0 & U_i^\pm \end{bmatrix} \\
B_i &= \begin{bmatrix} b_{11}^i & 0 \\ 0 & b_{22}^i \end{bmatrix} \\
C &= \begin{bmatrix} c_{11} & c_{12} \\ c_{21} & c_{22} \end{bmatrix}
\end{aligned}$$

$$U_i^\pm = \left(U_i \pm |U_i|\right)/2$$

$$\begin{aligned}
b_{11}^1 &= \frac{\mu_k}{J\,Re}\left(\xi_x^2 + \xi_y^2 + \xi_z^2\right)\delta_\xi\left(\frac{J}{\rho}\right) \\
b_{11}^2 &= \frac{\mu_k}{J\,Re}\left(\eta_x^2 + \eta_y^2 + \eta_z^2\right)\delta_\eta\left(\frac{J}{\rho}\right) \\
b_{11}^3 &= \frac{\mu_k}{J\,Re}\left(\zeta_x^2 + \zeta_y^2 + \zeta_z^2\right)\delta_\zeta\left(\frac{J}{\rho}\right) \\
b_{22}^i &= \frac{\mu_\epsilon}{\mu_k} b_{11}^i
\end{aligned}$$

$$\begin{aligned}
c_{11} &= \frac{1}{Re}\left[\frac{2\Pi}{\rho k} - 2\frac{\mu}{\rho y^2}\right] \\
c_{12} &= \frac{1}{Re}\left[\frac{-\Pi}{\rho\epsilon} - \left(1 + F(M_t)\right)Re\right] \\
c_{21} &= \frac{1}{Re}\left[\left(C_{\epsilon 1} f_1 \Pi + C_{\epsilon 2} f_2 \rho\epsilon Re\right)\frac{\epsilon}{\rho k^2}\right. \\
&\quad \left. -0.22\frac{4}{36}C_{\epsilon 2}\left(Re_t\frac{\epsilon}{k}\right)^2 exp\left(-\frac{Re_t^2}{36}\right)Re\right] \\
c_{22} &= \frac{1}{Re}\left[-2C_{\epsilon 2} f_2 \frac{\epsilon}{k} Re - 2\frac{\mu}{\rho y^2}\epsilon exp\left(-\frac{y^+}{2}\right)\right. \\
&\quad \left. +0.22\frac{2}{36}C_{\epsilon 2}\; Re_t^2\;\frac{\epsilon}{k}\; exp\left(-\frac{Re_t^2}{36}\right)Re\right]
\end{aligned}$$

The convection terms on the RHS are discretized using the Total Variation Diminishing (TVD) upwinding scheme of Gorski[10], which may be first, second, or third order accurate depending on the constants used. Because the convection terms contain first-order derivatives, they are similar to a system of linear hyperbolic equations. The use of a standard central-differencing scheme can result in nonphysical oscillations in the dependant variables, especially in regions of high gradients. The TVD property results in solutions which are essentially oscillation-free.

The scheme begins by representing the convective terms with numerical fluxes

$$\partial_\xi f \approx \frac{f_{i+1/2} - f_{i-1/2}}{\Delta\xi}$$

A first-order numerical flux is then defined as

$$h_{i+1/2} = \frac{1}{2}\left(f_{i+1} + f_i - df^+_{i+1/2} + df^-_{i+1/2}\right)$$

Second- and third-order fluxes are obtained by adding corrections to the first-order flux.

$$f_{i+1/2} = h_{i+1/2} \; -\tfrac{1-\phi}{4}\,\dot{df}^-_{i+3/2} - \tfrac{1+\phi}{4}\,\ddot{df}^-_{i+1/2} + \tfrac{1+\phi}{4}\,\dot{df}^+_{i+1/2} + \tfrac{1-\phi}{4}\,\ddot{df}^+_{i-1/2}$$

The symbols $\dot{df}$ and $\ddot{df}$ denote flux limited values of df and are computed using the minmod operators described by Chakravarthy [11]

$$\dot{df}^-_{i+3/2} = minmod\left(df^-_{i+3/2}, \beta \cdot df^-_{i+1/2}\right)$$
$$\ddot{df}^-_{i+1/2} = minmod\left(df^-_{i+1/2}, \beta \cdot df^-_{i+3/2}\right)$$
$$\dot{df}^+_{i+1/2} = minmod\left(df^+_{i+1/2}, \beta \cdot df^+_{i-1/2}\right)$$
$$\ddot{df}^+_{i-1/2} = minmod\left(df^+_{i-1/2}, \beta \cdot df^+_{i+1/2}\right)$$
$$minmod(x, y) = sign(x) \cdot max\left\{0, min\left[|x|, y \cdot sign(x)\right]\right\}$$

where the compression parameter, β, is defined as

$$\beta = \frac{3-\phi}{1-\phi}$$

Second- or third-order schemes can be obtained by setting ϕ equal to -1, or 1/3 respectively. Then, for example, the convective terms in the turbulent kinetic energy equation can be written as,

$$\begin{aligned} f &= \alpha \cdot k \\ \alpha &= J^{-1}\rho U \end{aligned}$$

and the flux differences are

$$df^+_{i+1/2} = max(\alpha_{i+1}, 0) \cdot k_{i+1} - max(\alpha_i, 0) \cdot k_i$$
$$df^-_{i+1/2} = min(\alpha_{i+1}, 0) \cdot k_{i+1} - min(\alpha_i, 0) \cdot k_i$$

For the convective terms in the $\eta-$ or $\zeta-$ directions, U is replaced by the appropriate contravarient velocity and i is replaced by the corresponding coordinate index.

Since the diffusion terms are composed of second-order derivatives, which tend to have a smoothing effect, oscillations in the dependent flow variables is not of concern and a standard central difference discretization can be used. For example, the diffusion of turbulent kinetic energy in the $\xi-$ direction is computed from

$$\partial_\xi g \approx \frac{\left(g_{i+1/2} - g_{i-1/2}\right)_{j,k}}{\triangle\xi}$$

where

$$\begin{aligned} g_{i+1/2,j,k} &= [\alpha \nabla\xi \cdot \nabla k]_{i+1/2,j,k} \\ &= [\alpha\left(\xi_x k_x + \xi_y k_y + \xi_z k_z\right)]_{i+1/2,j,k} \\ \alpha_{i+1/2,j,k} &= \left[\frac{1}{J\,Re}\left(\mu + \frac{\mu_t}{\sigma_k}\right)\right]_{i+1/2,j,k} \\ (k_x)_{i+1/2,j,k} &= (\xi_x k_\xi + \eta_x k_\eta + \zeta_x k_\zeta)_{i+1/2,j,k} \\ (k_y)_{i+1/2,j,k} &= (\xi_y k_\xi + \eta_y k_\eta + \zeta_y k_\zeta)_{i+1/2,j,k} \\ (k_z)_{i+1/2,j,k} &= (\xi_z k_\xi + \eta_z k_\eta + \zeta_z k_\zeta)_{i+1/2,j,k} \end{aligned}$$

and μ and μ_t at $i+1/2$ are computed from a simple average between i and $i+1$. To determine the gradient of k in the sweep direction,

$$(k_\xi)_{i+1/2,j,k} = (k_{i+1} - k_i)_{j,k}$$

and for the non-sweep directions,

$$\begin{aligned} (k_\eta)_{i+1/2,j,k} &= \frac{1}{2}\left[(k_\eta)_i + (k_\eta)_{i+1}\right]_{j,k} \\ (k_\zeta)_{i+1/2,j,k} &= \frac{1}{2}\left[(k_\zeta)_i + (k_\zeta)_{i+1}\right]_{j,k} \\ (k_\eta)_{i,j,k} &= \frac{1}{2}\left(k_{j+1} - k_{j-1}\right)_{i,k} \\ (k_\zeta)_{i,j,k} &= \frac{1}{2}\left(k_{k+1} - k_{k-1}\right)_{i,j} \end{aligned}$$

The convection terms on the LHS are discretized using a flux-splitting technique and the diffusion terms are discretized using a second order central difference. By neglecting the cross-derivative terms that would normally appear in B_i, the resulting equations form a block tridiagonal system which can be readily inverted.

Initialization

The turbulent transport variables for the Chien $k-\epsilon$ model (k, ϵ, μ_t) can be initialized using two different techniques. The preferred method uses an assumption of turbulent equilibrium, in which the production of turbulent kinetic energy equals the rate of dissipation, together with an existing turbulent viscosity profile to initialize the k and ϵ variables.

$$\begin{aligned} \rho\epsilon &= \Pi/Re \\ \rho k &= \sqrt{\frac{\rho\epsilon\mu_t}{C_\mu f_\mu Re}} \end{aligned}$$

In order to use this technique, the code must first be run a few thousand iterations using another eddy-viscosity turbulence model. Initializing from

an existing turbulent viscosity profile rather than uniform values aids somewhat in convergence and improves the stability of the model by reducing the severe changes in turbulence values that occur during the first few iterations after initialization.

The second method initializes the turbulence variables to uniform values (k, ϵ, μ_t) within each zone using the local density. This technique has not been found to be very robust.

Stability Enhancements

Relaxation

Updated values of k, ϵ, and μ_t are relaxed for a set number of iterations following initialization. Relaxation of these variables reduces the amount they may change during any single iteration. Immediately after initialization, the allowed changes are significantly reduced. This restriction is then gradually lifted as the last relaxation iteration is approached.

Limiters

The $k-\epsilon$ model also uses limiters within the interior of each zone to increase convergence and stability by capping the values of the turbulence quantities at both the high and low extremes. This is usually only necessary during the first few iterations after initialization, when the fluctuations in k and ϵ tend to be the most severe.

Nondimensional values of the minimum limiters have been preset to relatively small numbers. The values of the maximum limiters are determined by user inputs for the maximum allowable turbulent viscosity $\mu_{t\,max}$ and a turbulent reference velocity, from which the maximum allowable value for the turbulent kinetic energy is computed using:

$$k_{max} = 0.10 \frac{u^2_{ref(k-\epsilon)}}{2}$$

The maximum dissipation rate is computed from the turbulent viscosity relation.

The use of these limiters can be summarized as follows: (1) If either k or ϵ falls below preset minimum values then both are reset to these values. This typically occurs in the freestream. (2) If the turbulent kinetic energy exceeds k_{max}, then it is capped at this value. The dissipation rate is taken to be the larger of the current dissipation rate or ϵ_{max}. (3) If the turbulent viscosity exceeds $\mu_{t\,max}$, then it is capped at this value and the turbulent kinetic energy is recomputed from the turbulent viscosity relation. The turbulent dissipation rate is left unchanged.

These maximum limiters are meant to keep the solution from diverging during the initial iterations of the solution and care must be taken that these limiters are not constraining the solution upon final convergence. Verifying that the maximum value of the turbulent viscosity in the flowfield is less than that specified for $\mu_{t\,max}$ is usually sufficient. At the conclusion of a set of iterations, the WIND code provides the user with a warning message if the solution is being constrained by the maximum limiters.

Variable C_μ

It is well known that the baseline $k-\epsilon$ model is poorly suited to adverse pressure gradient flows. Rodi and Scheuerer[12] demonstrated that for these types of flows, the rate of dissipation near solid boundaries is too small relative to the rate of production of turbulent kinetic energy. This causes the model to overpredict skin friction and predict flows to be attached when experimental results show them to be separated. The variable C_μ formulation, which is derived from algebraic stress modeling, is designed to help remedy this problem by reducing the turbulent viscosity in regions of the flowfield where the production of turbulent kinetic energy is significantly larger than the rate of dissipation. The specific formulation used is taken from Rodi[13]:

$$C_\mu = min\left(0.09, \frac{0.10738\,(0.64286 + 0.19607R)}{[1 + 0.357\,(R-1)]^2}\right)$$

As the ratio R of production to dissipation increases above one, the coefficient C_μ is reduced from its normal value of 0.09 to limit the turbulent viscosity.

The variable C_μ option also provides added stability to the $k-\epsilon$ model , such as in the case of an airfoil, where the sudden deceleration of the flow near the leading edge would otherwise result in an unrealistically high rate of production. In regions of the flow where the turbulence is in equilibrium, i.e. where the production and dissipation are balanced, the turbulent viscosity remains unchanged.

Numerical Results

The focus of this validation effort will be on wall-bounded flows. For a similar code to code comparison of mixing results for supersonic exhaust nozzles, the reader is referred to reference 14.

Flat Plate

The incompressible flow over a smooth flat plate was used as an initial validation case. The flow being modeled is that reported by Wieghardt[15] and later included in the 1968 AFOSR-IFP Stanford Conference[16]. The freestream Mach number in the simulations was set to 0.20, slightly higher than that in the experiment, in order to accelerate the convergence rate.

Figure 1 depicts the computational domain used to model this flow. A Cartesian mesh with 111 points in the axial direction and 81 points normal to the viscous wall was used. The first 14 grid points upstream of the leading edge of the plate were treated as an inviscid wall to provide a uniform profile at the leading edge location. The grid was packed in the streamwise direction to resolve flow gradients near the leading edge of the plate and normal to the surface to resolve the boundary layer. Calculations were made on a series of grids having y^+ values of 1, 2, 5, 10, and 30 at the first point off the wall. Figure 2 indicates that these values are representative of the maximum y^+ along the plate as computed from the WIND $k-\epsilon$ solutions. These grids are the same ones used in the Chien $k-\epsilon$ grid sensitivity study of reference 17 with the NPARC code.

Figure 3 shows the computed skin friction using both codes. The grid sensitivity studies shown in Figures 3a and 3b for the NPARC and WIND $k-\epsilon$ models indicate that grid independence for both codes is obtained using the $y^+ = 2$ grid. Figure 3c shows this to be the case for the WIND SST model as well. While the WIND skin friction results for larger y^+ values appear to be much less sensitive than the NPARC results, analysis of the turbulence quantities in the near-wall region reveal that the model predictions begin to break down severely as the mesh spacing exceeds $y^+ = 5$. Figure 3d is a direct comparison of the skin friction results between codes using the $y^+ = 1$ grid. As can be seen, the WIND $k-\epsilon$ results are improved and compare well with the WIND results using the SST model. The comparison of the computed velocity profiles at several axial stations given in Figure 4 also shows that the WIND code matches the experimental data quite well.

Examination of the turbulence quantities at the last velocity station ($Re_x = 1.03x10^7$) is given in Figures 5-7. Figure 5 compares the turbulent kinetic energy with the "average" experimental data assembled by Patel, Rodi, and Scheuerer[4]. While neither code matches this data exactly, the WIND results more closely match those obtained by Patel using the Chien model in a two-dimensional boundary layer code. The WIND SST model fails to capture the peak in the turbulent kinetic energy due to the form of the $k-\omega$ model used in the near-wall region. From the turbulent dissipation rate shown in Figure 6, one can see that the WIND results approach the correct limiting value away from the wall. Comparison of the turbulent shear stress in Figure 7 shows that only the WIND results approach the correct asymptotic value away from the wall.

Backstep

The second validation case is the incompressible flow over a backward facing step. As shown in Figure 8, this geometry has a step height to tunnel exit height ratio of 1:9 which helps to minimize the freestream pressure gradient due to sudden expansion. The experimental configuration of Driver and Seegmiller[18] also had a step height to tunnel width ratio of 1:12 to minimize three-dimensional effects. A variety of experimental measurements are available, including skin friction, pressure, turbulent normal and shear stresses, and velocity profiles downstream of the step.

A 238 x 185 single-zone mesh was generated to model the region from x/H = -105 to +50. The grid was packed to the solid surfaces such that $y^+ \approx 1$. Downstream of the step, 55 points were used in the recirculation region with ten of them placed within $y^+ \approx 30$. The grid was also clustered in the streamwise direction near the recirculation region to improve resolution.

Figure 9 shows the velocity profiles at several axial locations. Upstream of the step, all of the solutions are virtually identical. Within the recirculation region, however, there are noticable differences. The NPARC and WIND $k-\epsilon$ solutions are nearly indistinguishible and appear to provide the best match to the experimental data. Use of the variable C_μ option in the WIND $k-\epsilon$ model causes the flow to reattach further downstream, but does not predict the rest of the velocity profile as well as the standard $k-\epsilon$ model. The WIND SST model shows the greatest disparity compared to the data and predicts the flow to reattach even further downstream than the $k-\epsilon$ model with the variable C_μ option.

These findings relative to the extent of the recirculation region are reiterated in Figure 10, which shows the predicted skin friction coefficient. Both the NPARC and WIND $k-\epsilon$ models predict the reattachment to occur too far upstream and

display under- and overshoots relative to the data. According to Avva, Smith and Singhal[19] this overshoot can be reduced by increasing the number of points below $y^+ \approx 30$. For a mesh with ten points inside this region, the present results agree with those presented by Avva. The variable C_μ option tends to reduce the turbulent viscosity within the separation region, thus making the flow appear more laminar-like and reducing the magnitude of the skin friction. The predicted reattachment location is also shown to move downstream. Unlike for the velocity profiles, the WIND SST model seems to provide relatively good agreement with the skin friction data. Table 2 lists the reattachment location predicted by each model.

Table 2: Predicted Reattachment Locations for the Backward-Facing Step.

Model	x_r/H
NPARC $k-\epsilon$	5.31
WIND $k-\epsilon$	5.30
WIND $k-\epsilon$ Var. C_μ	5.55
WIND SST	6.43
Driver Experiment	6.26

Figure 11 shows the turbulent kinetic energy profiles at several axial locations. Upstream of the backstep, the flow is similar to that of the flat plate and one can again see that the peak value in turbulent kinetic energy is underpredicted by the SST model due to the form of the $k-\omega$ model used in the near-wall region. This difference appears to propagate downstream as the SST model consisently predicts a lower peak value than the $k-\epsilon$ model at each axial station. As with the velocity profiles of Figure 9, there is close agreement between the NPARC and WIND $k-\epsilon$ solutions. One can also notice the reduction in turbulent kinetic energy, especially within the recirculation region, caused by the use of the variable C_μ option. This occurs because the variable C_μ option effectively increases the turbulent dissipation rate within the recirculation zone.

The corresponding Reynolds stress profiles are shown in Figure 12. Here again there is excellent agreement between the NPARC and WIND $k-\epsilon$ solutions, except near x/H=0 where the WIND solution predicts a more rapid increase in the downward component of velocity. Far downstream the $k-\epsilon$ model overpredicts the Reynolds stress which corresponds with the overprediction in skin friction shown in Figure 10. One can also observe how the variable C_μ correction noticeably reduces the peak turbulent viscosity (and consequently the Reynolds stress) within the recirculation region. The ability of the SST model to match the Reynolds stress data so well downstream of the reattachment location is interesting, considering the underprediction of velocity and turbulent kinetic energy in this same region.

Transonic Diffuser

The Sajben[20, 21] diffuser strong-shock case was selected as the next validation case. Figure 13 is a schematic of the two-dimensional diffuser geometry. This configuration had an entrance to throat area ratio of 1.4, an exit to throat area ratio of 1.5, and a sidewall spacing of approximately four throat heights. Suction slots were placed on the side walls of the constant area sections upstream and downstream of the diffuser to minimize three-dimensional effects. Streamwise slots were also placed along the top corners of the diffuser to maintain a two-dimensional flow. Time-averaged static pressure distributions on the top and bottom diffuser walls were measured using pressure transducers, and separation and reattachment locations were obtained through the use of oil-flow techniques. Velocity profiles were obtained using a laser Doppler velocimeter.

Although this geometry was tested both with and without externally applied oscillations, only the steady-state flow of the unexcited cases was modeled numerically. These flows were characterized by the ratio of exit static to inflow total pressure. For the strong-shock case this ratio was 0.72.

This case was computed using an 81 x 51 grid, which corresponds to the coarse mesh used in the investigation conducted by Georgiadis, Drummond and Leonard[22] with the PARC code. They found the grid to be sufficiently clustered in the vertical direction such that the first point off the wall resided inside the laminar sublayer.

Figure 14 shows that without any turbulence model corrections, the WIND $k-\epsilon$ model predicts the shock too far downstream and poorly matches the pressure distributions downstream of the shock. Use of the Sarkar compressibility correction improves the prediction of the shock location somewhat, but does not improve the flowfield solution in the downstream region. The variable C_μ option has the same effect on the shock location as the Sarkar correction, but also improves the downstream pressure predictions. By using the Sarkar correction in conjunction with the variable C_μ option, the shock location is reasonably well matched and the downstream pressure distribution is improved.

Figure 15 illustrates the effect of the $k-\epsilon$ model correction factors on the predicted velocity profiles downstream of the shock. Without any corrections, the model is unable to match the experimental data near the lower wall and the core flow velocity is underpredicted. Use of either the Sarkar compressibility correction or the variable C_μ option yields improved results both near the walls and in the core. Using both correction factors yields some additional improvement near the lower wall, while the upper wall region appears to be over-corrected.

Cross-code comparisons of the strong shock results are made in Figures 16 and 17. Two sets of WIND $k-\epsilon$ results are plotted. The first set uses the same correction factors (Sarkar compressibility correction used, but not the variable C_μ option) as the NPARC code and should be used to compare the new and old $k-\epsilon$ implementations. The second series was computed using both correction factors to demonstrate the benefit of using the variable C_μ option. Figure 16 shows that the WIND and NPARC $k-\epsilon$ model pressure distributions are again in close agreement, with the WIND code still predicting the shock location one or two grid points further downstream. With the addition of the variable C_μ option, the shock location predicted using WIND agrees well with that using NPARC and the downstream pressure distribution compares better with the experimental data. The WIND SST model also provides improved downstream pressure distributions, but predicts the shock to occur further upstream than indicated by the experimental data.

Conclusion

The two-equation Chien $k-\epsilon$ turbulence model has been successfully implemented in the WIND Navier-Stokes flow solver. Details of the numerical algorithm have been presented including the initialization procedure, stability enhancements, compressibility corrections, and variable C_μ formulation. Results for the wall-bounded flows investigated herein indicate that the current implementation functions very similarly to that in the NPARC code, though the WIND code appears to be slightly more accurate in predicting skin friction at the wall. Comparison of the Chien model results with those from the SST model for these cases yielded no obvious favorite.

References

1. Bush, R. H., Power, G. D., and Towne, C. E., "WIND: The Production Flow Solver of the NPARC Alliance," AIAA Paper 98-0935, Jan. 1998.

2. Menter, F. R., "Improved Two-Equation $k-\omega$ Turbulence Models for Aerodynamic Flows," NASA TM-103975, Oct. 1992.

3. Chien, K.-Y., "Predictions of Channel and Boundary-Layer Flows with a Low Reynolds Number Turbulence Model," *AIAA Journal*, Vol. 20, No. 1, Jan. 1982, pp. 33-38.

4. Patel, V. C., Rodi, W., and Scheuerer, G., "Turbulence Models for Near-Wall and Low-Reynolds Number Flows: A Review," *AIAA Journal*, Vol. 23, No. 9, Sept. 1985, pp. 1308-1319.

5. Wilcox, D. C., "Comparison of Two-Equation Turbulence Models for Boundary Layers with Pressure Gradient," *AIAA Journal*, Vol. 31, No. 8, Aug. 1993, pp. 1414-1421.

6. Nichols, R. H., "A Two-Equation Model for Compressible Flows," AIAA Paper 90-0494, Jan. 1990.

7. Georgiadis, N. J., Chitsomboon, T., and Zhu, J., "Modification of the Two-Equation Turbulence Model in NPARC to a Chien Low Reynolds Number $k-\epsilon$ Formulation," NASA TM-106710, Sept. 1994.

8. Sarkar, S., Erlebacher, G., and Kreiss, H. O., "The Analysis and Modeling of Dilatational Terms in Compressible Turbulence," *Journal of Fluid Mechanics*, Vol. 227, 1991, pp. 473-493.

9. Wilcox, D., "Dilatation-Dissipation Corrections for Advanced Turbulence Models," *AIAA Journal*, Vol. 30, No. 11, Nov. 1992, pp. 2639-2646.

10. Gorski, J. J., Chakravarthy, S. R., and Goldberg, U. C., "High Accuracy TVD Schemes for the k-e Equations of Turbulence," AIAA Paper 85-1665, July 1985.

11. Chakravarthy, S. R., Ssema, K. Y., Goldberg, U. C., Gorski, J. J., and Osher, S., "Application of a New Class of High Accuracy TVD Schemes to the Navier-Stokes Equations," AIAA Paper 85-0165, Jan. 1985.

12. Rodi, W. and Scheuerer, G., "Scrutinizing the $k-\epsilon$ Turbulence Model Under Adverse Pressure Gradient Conditions," *Transactions of the ASME, Journal of Fluids Engineering*, Vol. 108, 1986, pp. 174–179.

13. Rodi, W., "A New Algebraic Relation for Calculating the Reynolds Stresses," *Z. Ang. Math. Mech.*, Vol. 56, 1976, pp. T219–T221.

14. Georgiadis, N. J., Yoder, D. A., and DeBonis, J. R., "A Comparison of Three Navier-Stokes Solvers for Exhaust Nozzle Flowfields," AIAA Paper 99–0748, Jan. 1999.

15. Wieghardt, K. and Tillman, W., "On the Turbulent Friction Layer for Rising Pressure," NACA TM-1314, 1951.

16. Coles, D. E. and Hirst, E. A., editors, *Computation of Turbulent Boundary Layers-1968 AFOSR-IFP-Stanford Conference*, Vol. 2, Stanford University, CA, 1969.

17. Georgiadis, N. J., Dudek, J. C., and Tierney, T. P., "Grid Resolution and Turbulent Inflow Boundary Condition Recommendations for NPARC Calculations," NASA TM–106959, July 1995.

18. Driver, D. M. and Seegmiller, H. L., "Features of a Reattaching Turbulent Shear Layer in Divergent Channel Flow," *AIAA Journal*, Vol. 23, No. 2, Feb. 1985, pp. 163–171.

19. Avva, R. K., Smith, C. E., and Singhal, A. K., "Comparative Study of High and Low Reynolds Number Versions of $k-\epsilon$ Models," AIAA Paper 90–0246, Jan. 1990.

20. Sajben, M. and Kroutil, J. C., "Effects of Initial Boundary-Layer Thickness on Transonic Diffuser Flows," *AIAA Journal*, Vol. 19, No. 11, Dec. 1981, pp. 1386–1393.

21. Salmon, J. T., Bogar, T. J., and Sajben, M., "Laser Doppler Velocimeter Measurements in Unsteady, Separated, Transonic Diffuser Flows," *AIAA Journal*, Vol. 21, No. 12, Dec. 1983, pp. 1690–1697.

22. Georgiadis, N. J., Drummond, J. E., and Leonard, B. P., "Evaluation of Turbulence Models in the PARC Code for Transonic Diffuser Flows," NASA TM–106391, Jan. 1994.

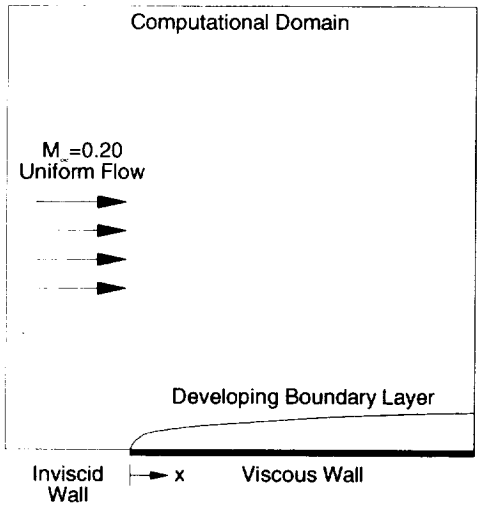

Figure 1: Schematic of the Flat Plate Test Case.

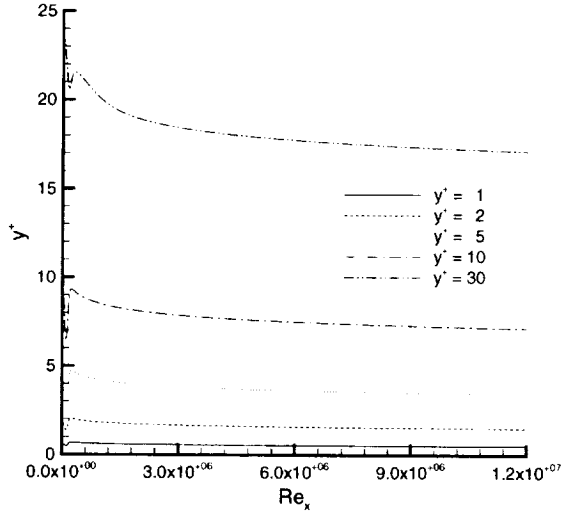

Figure 2: Near-Wall Grid Spacing for Flat Plate Case.

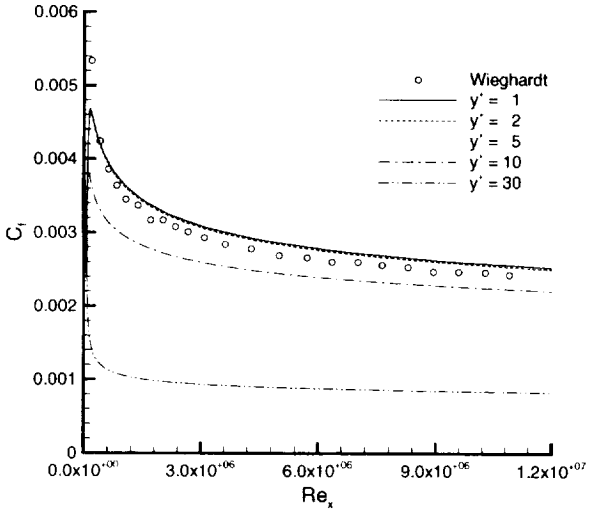

Figure 3a: NPARC Chien k-ε Grid Sensitivity Study.

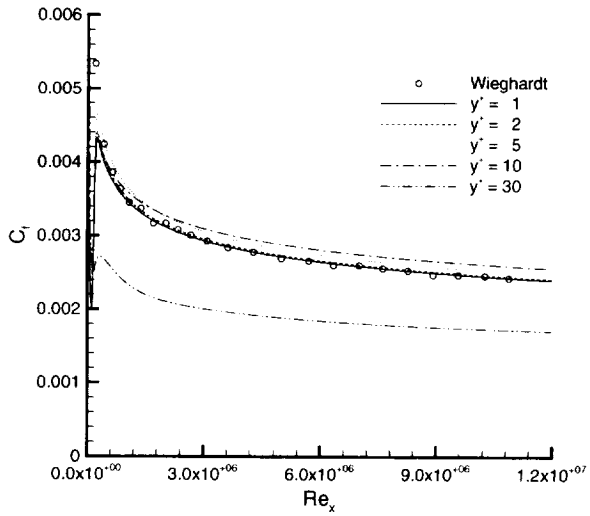

Figure 3b: WIND Chien k-ε Grid Sensitivity Study.

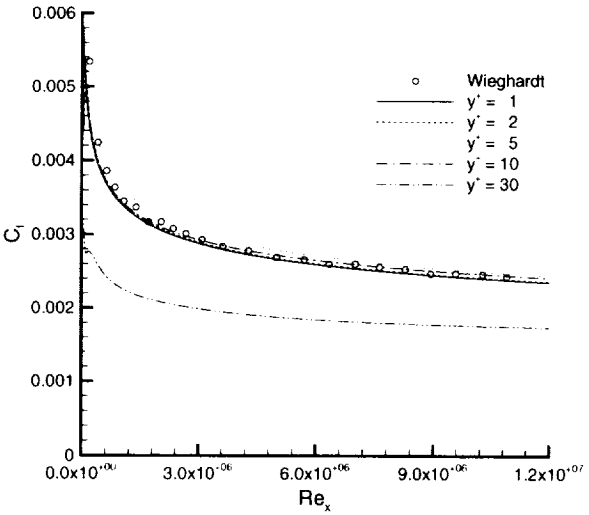

Figure 3c: WIND SST Grid Sensitivity Study.

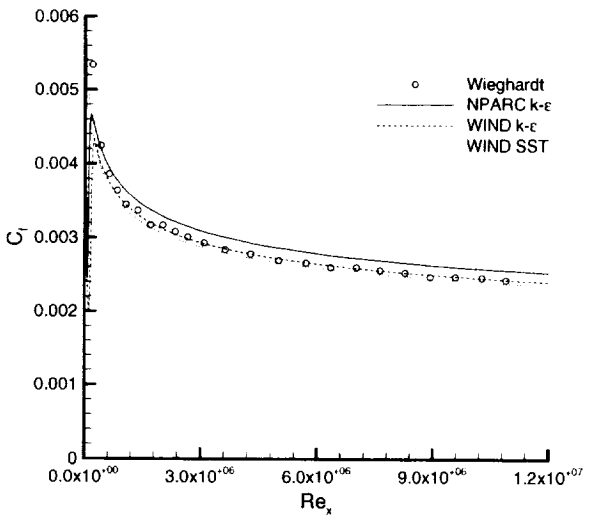

Figure 3d: Comparison of Grid Independent Solutions.

Figure 3: Local Skin Friction Along Flat Plate.

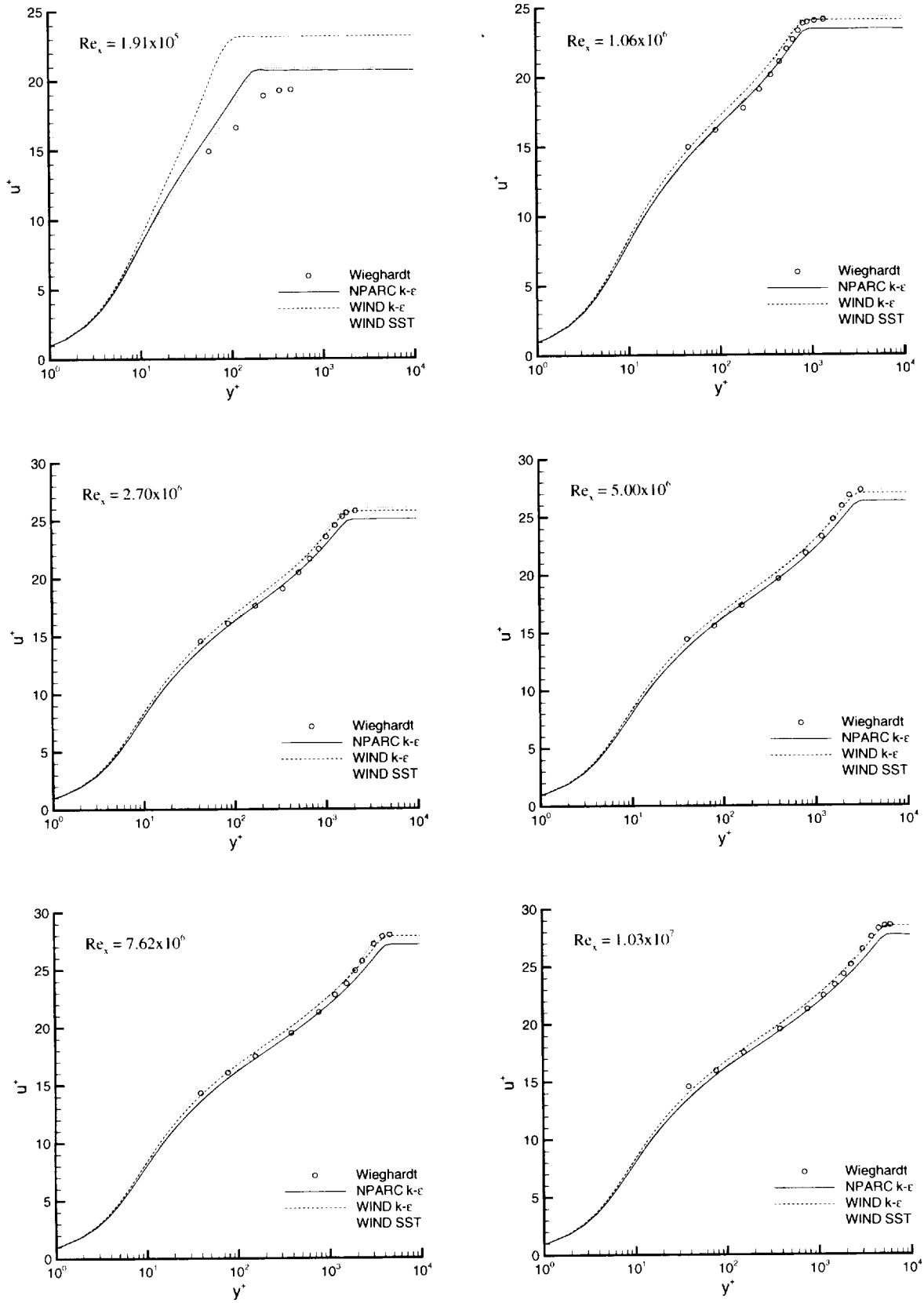

Figure 4: Velocity Profiles Along Flat Plate Using y^+=1 Grid.

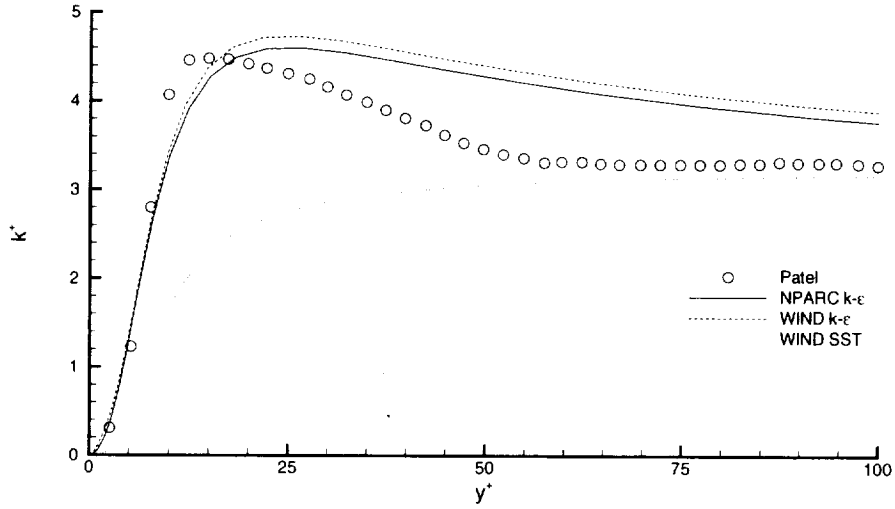

Figure 5: Turbulent Kinetic Energy Profiles in Near-Wall Region.

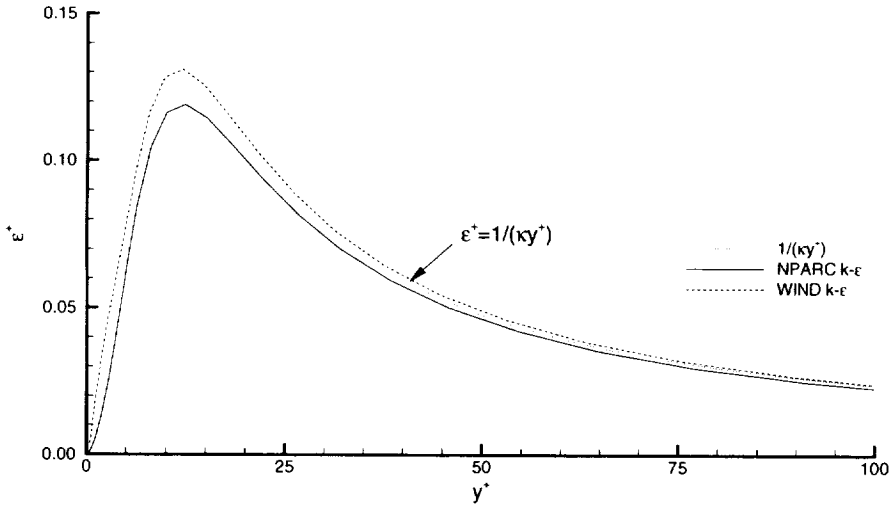

Figure 6: Turbulent Dissipation Rate in Near-Wall Region.

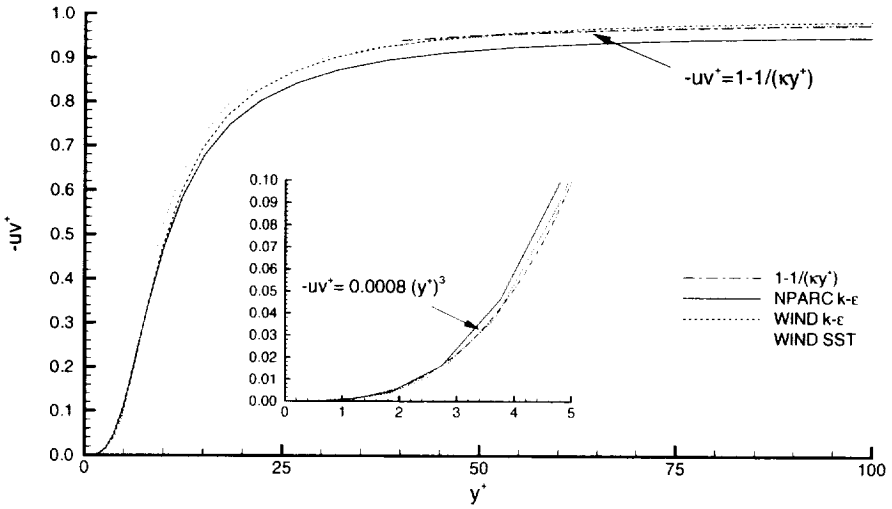

Figure 7: Reynolds Stress in Near-Wall Region.

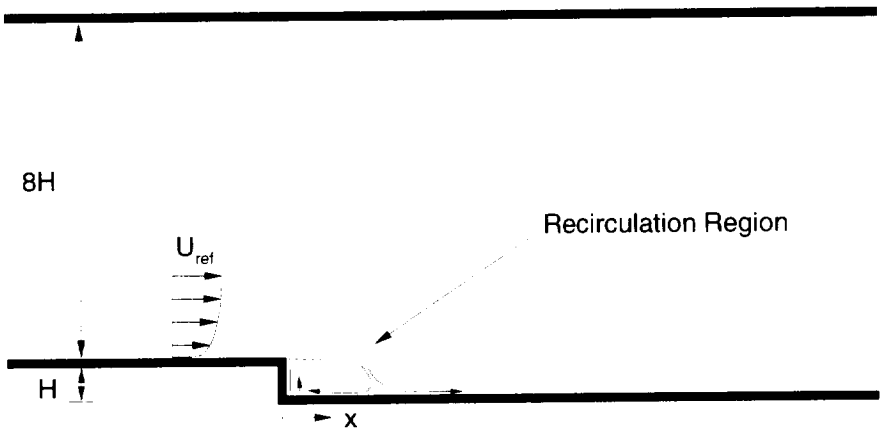

Figure 8: Schematic of Backward-Facing Step.

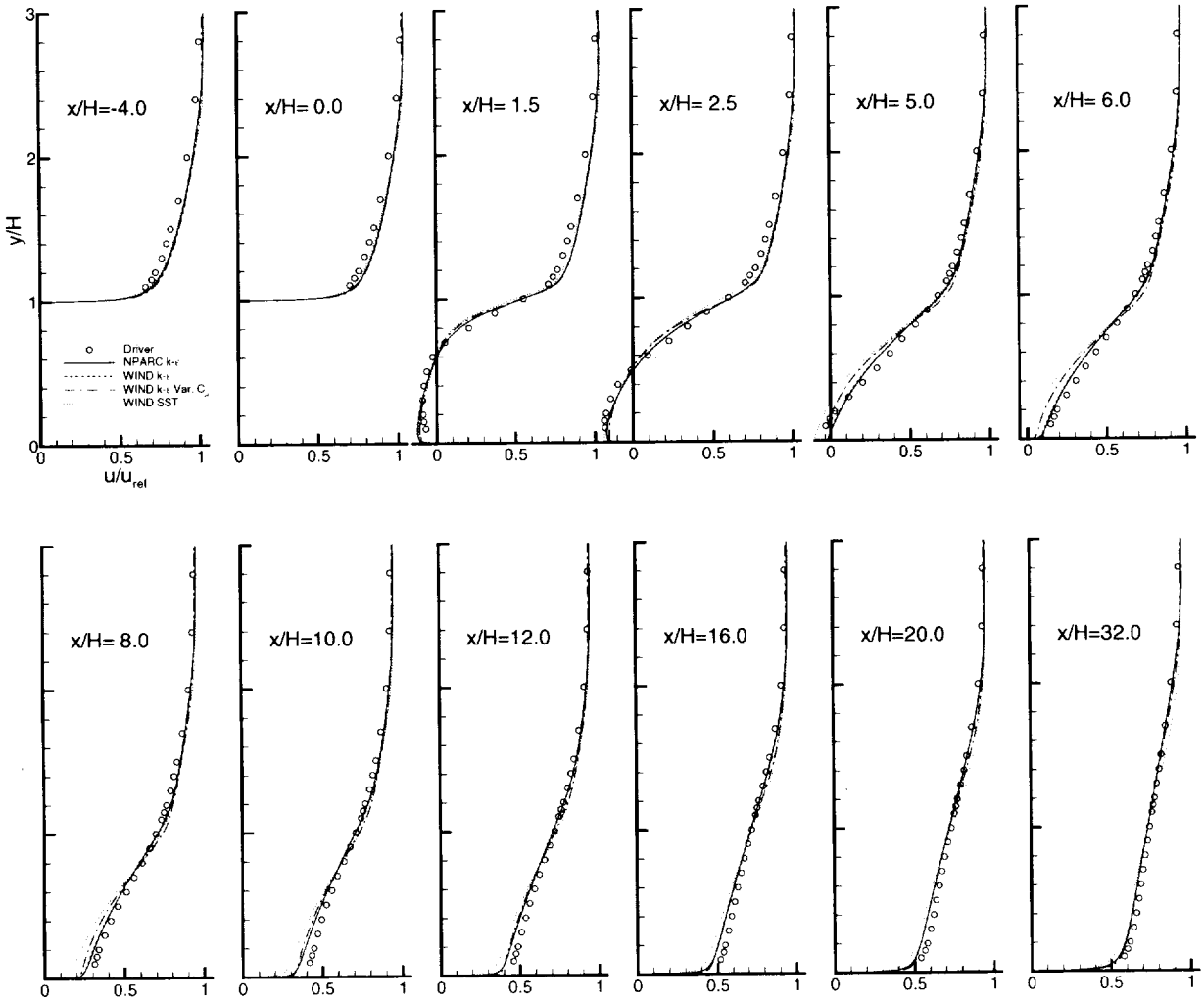

Figure 9: Velocity Profiles for Backward-Facing Step.

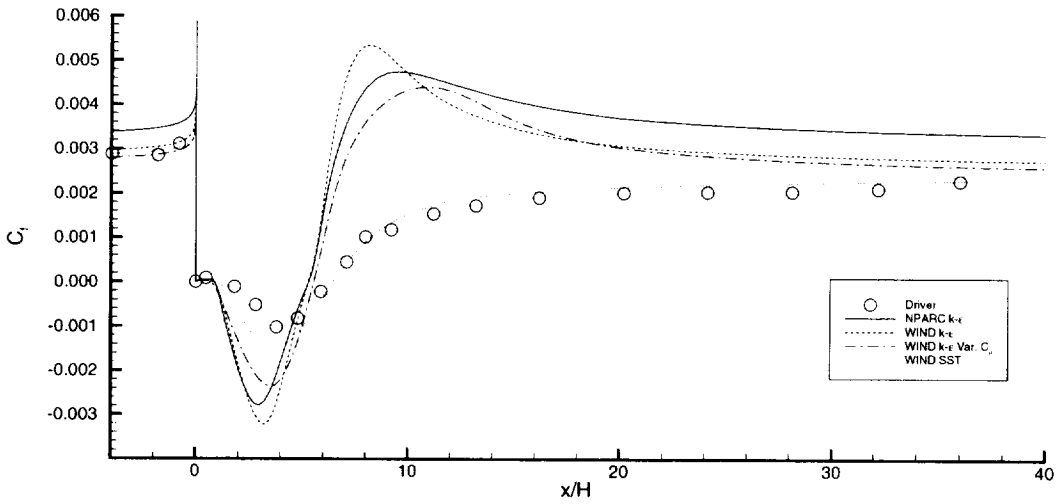

Figure 10: Local Skin Friction Coefficient Downstream of Backstep.

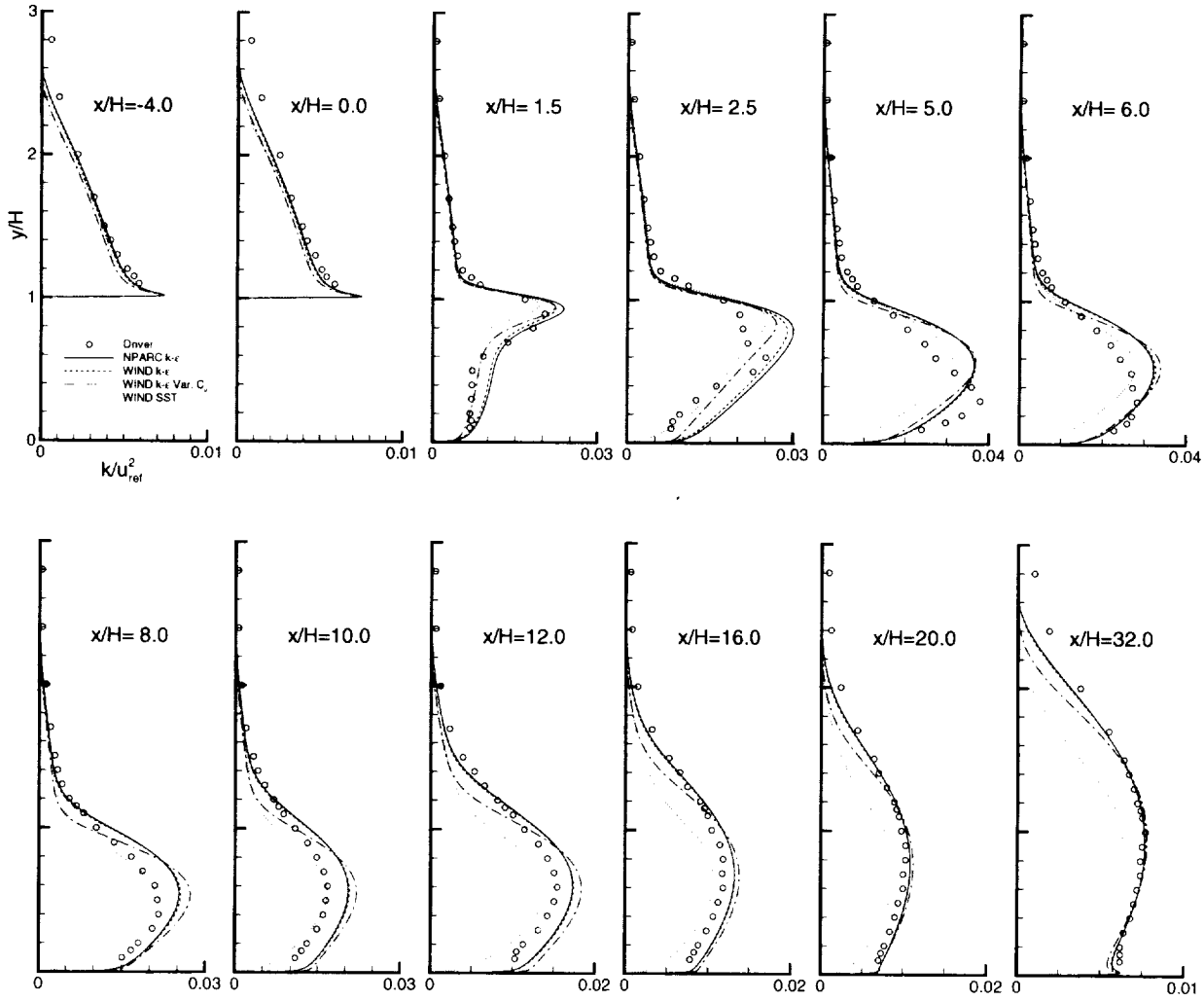

Figure 11: Turbulent Kinetic Energy Profiles for Backward-Facing Step.

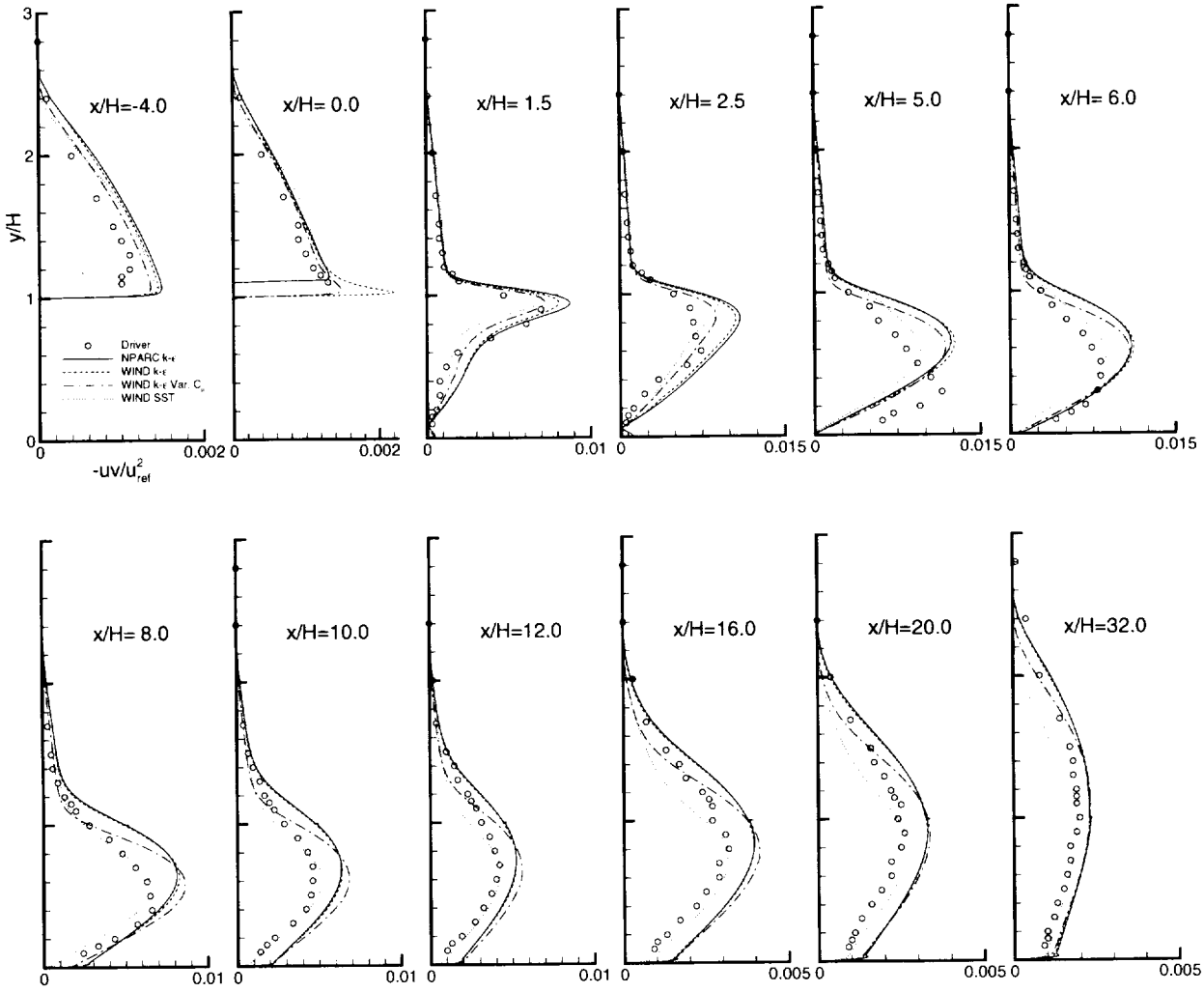

Figure 12: Reynolds Stress Profiles for Backward-Facing Step.

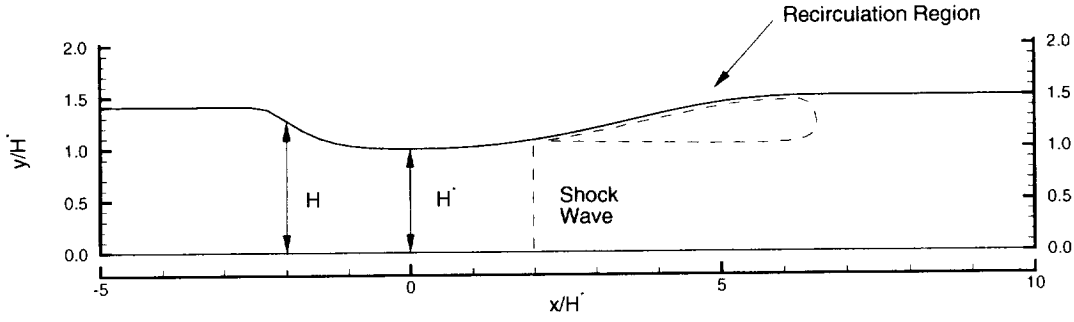

Figure 13: Schematic of Transonic Diffuser Test Case.

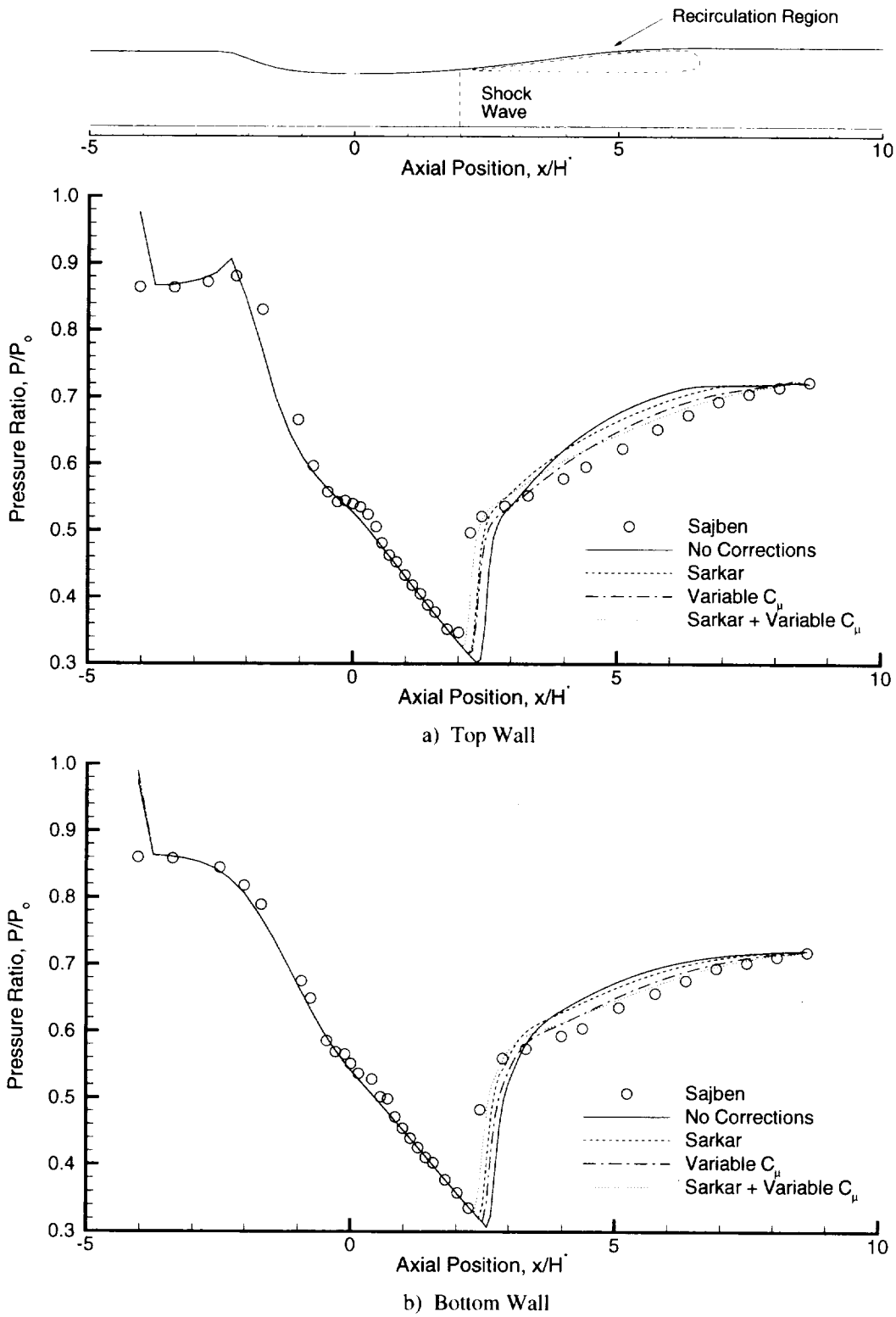

Figure 14: Effect of WIND k-ε Model Corrections on Predicted Pressure Distributions for the Transonic Diffuser Case.

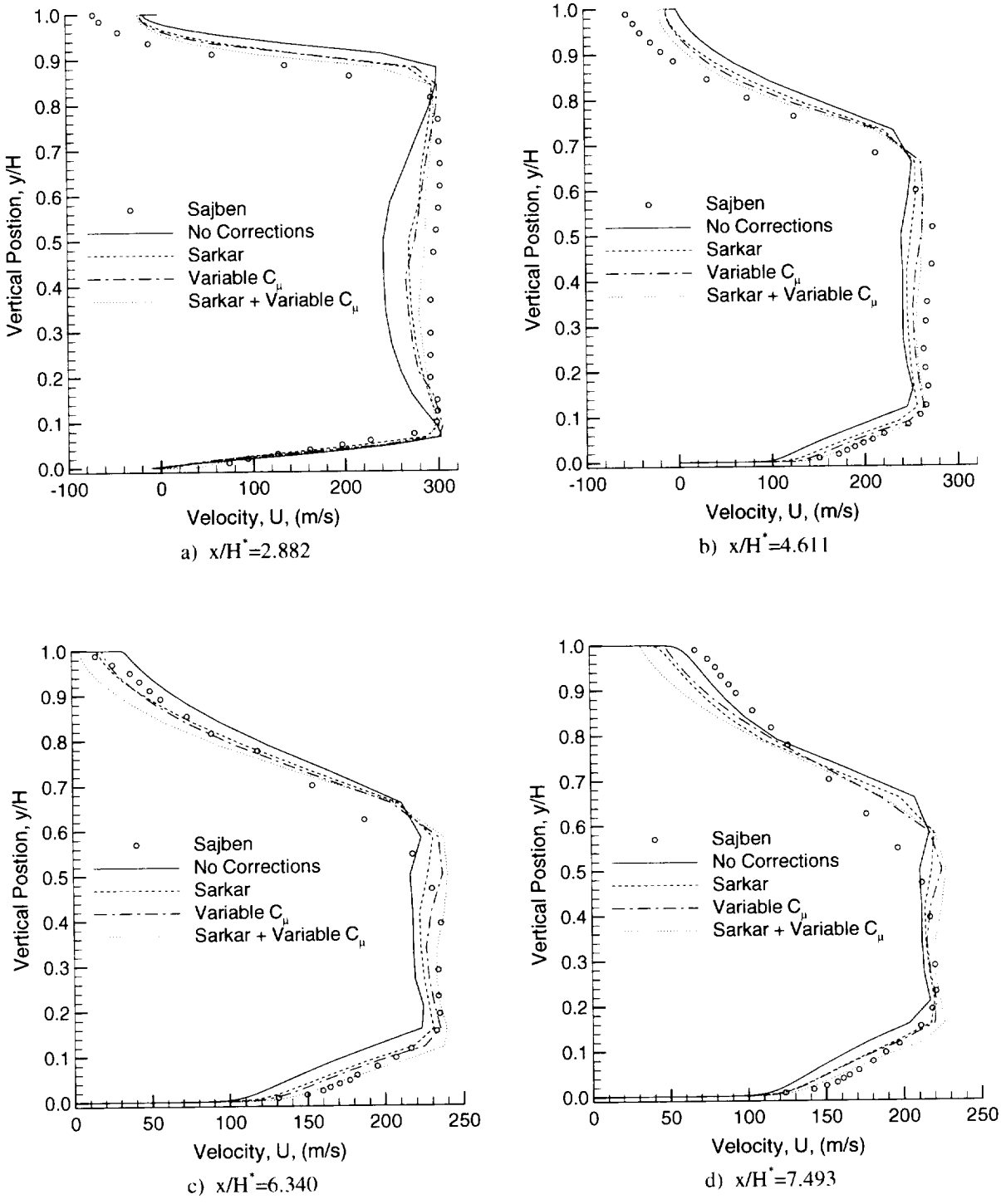

Figure 15: Effect of WIND k-ε Model Corrections on Predicted Velocity Profiles for the Transonic Diffuser Case.

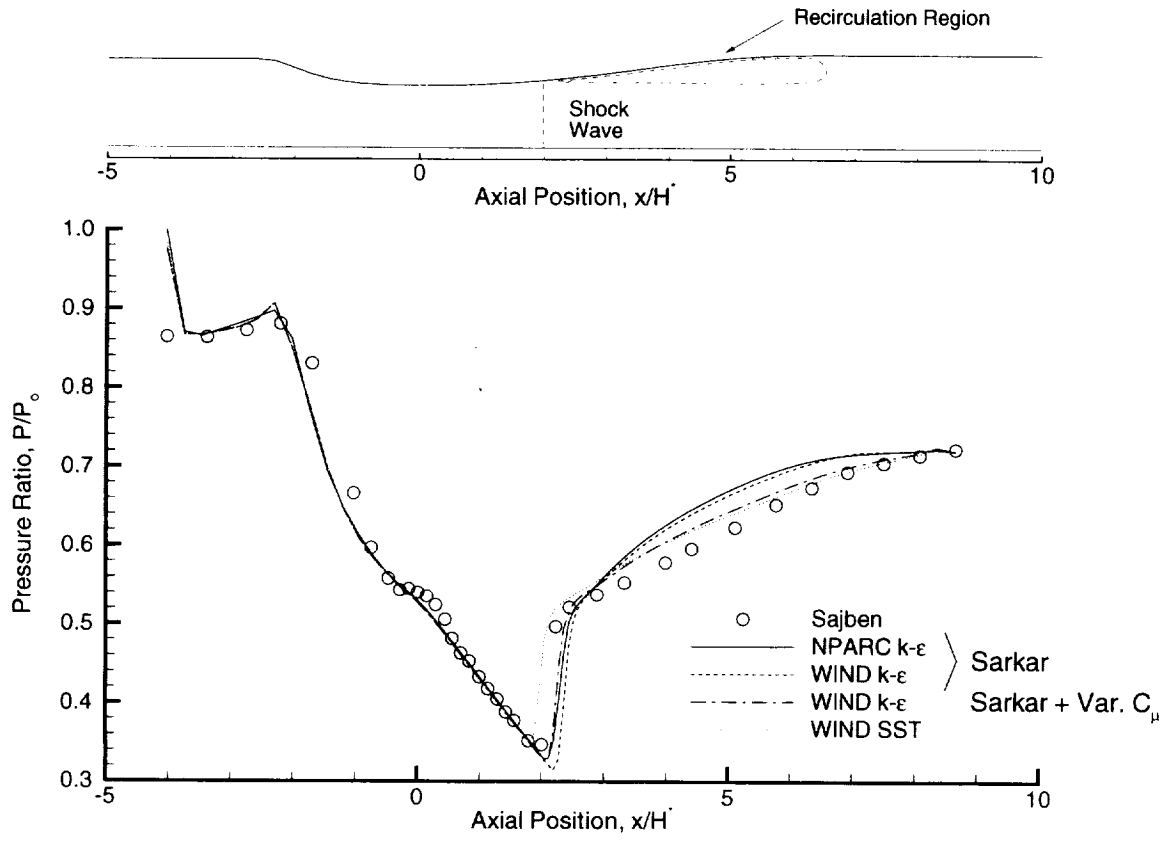

a) Top Wall

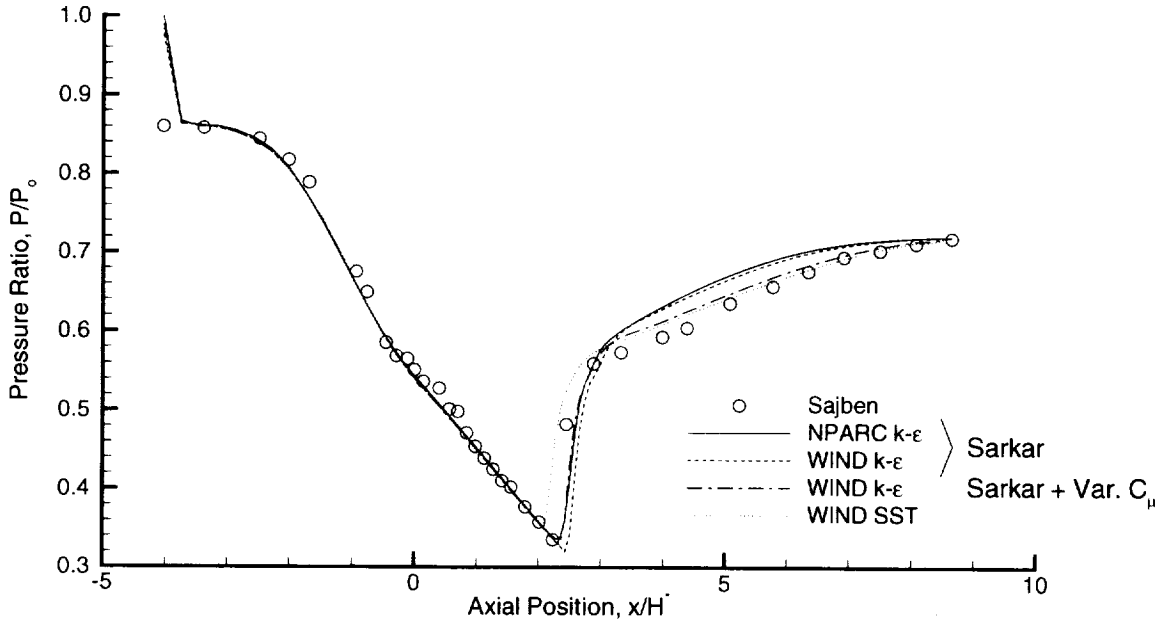

b) Bottom Wall

Figure 16: Pressure Distributions Along Top and Bottom Walls for the Transonic Diffuser Case.

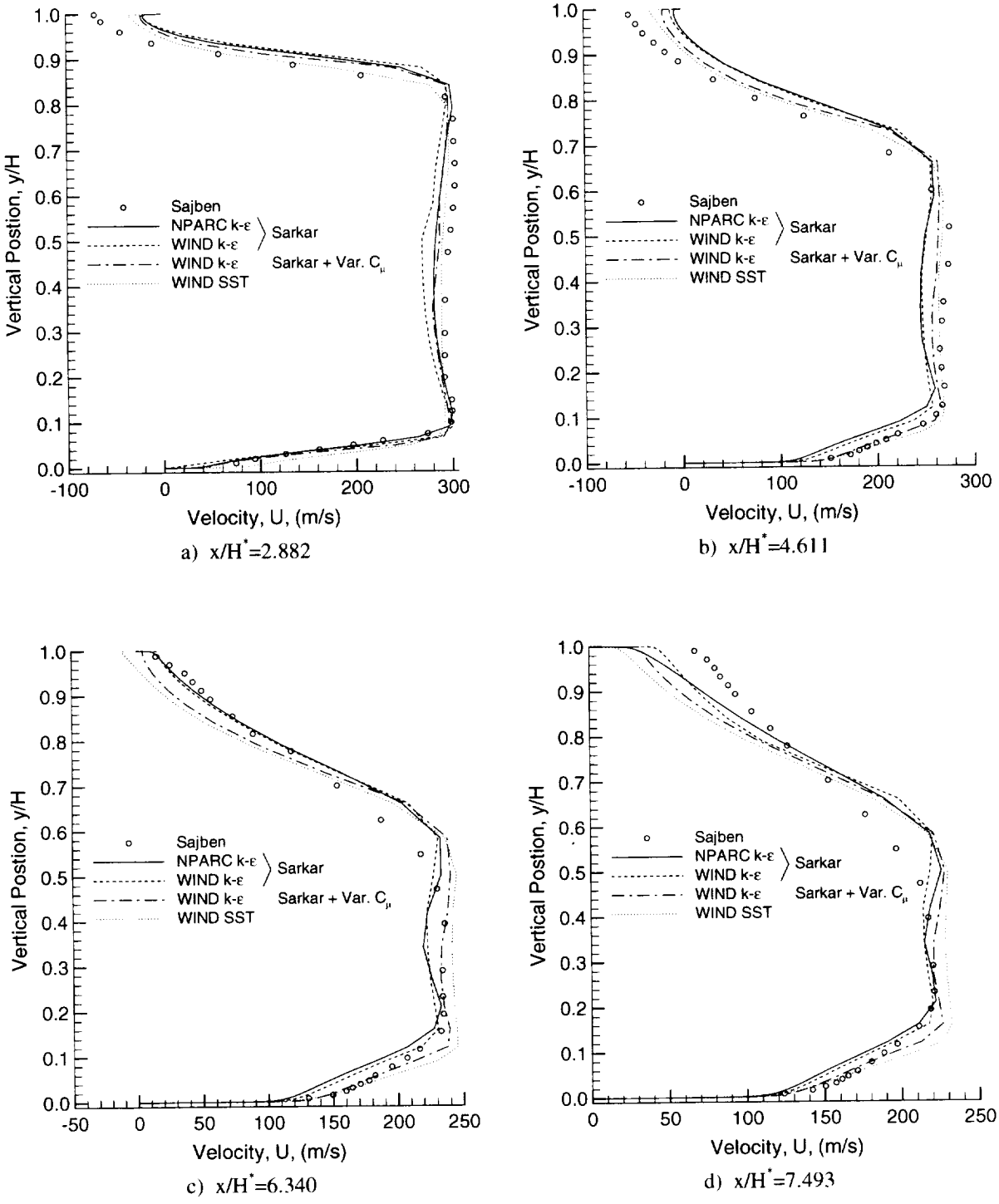

Figure 17: Velocity Profiles at Four Axial Locations for the Transonic Diffuser Case.

REPORT DOCUMENTATION PAGE

Form Approved
OMB No. 0704-0188

Public reporting burden for this collection of information is estimated to average 1 hour per response, including the time for reviewing instructions, searching existing data sources, gathering and maintaining the data needed, and completing and reviewing the collection of information. Send comments regarding this burden estimate or any other aspect of this collection of information, including suggestions for reducing this burden, to Washington Headquarters Services, Directorate for Information Operations and Reports, 1215 Jefferson Davis Highway, Suite 1204, Arlington, VA 22202-4302, and to the Office of Management and Budget, Paperwork Reduction Project (0704-0188), Washington, DC 20503.

1. AGENCY USE ONLY (*Leave blank*)	2. REPORT DATE	3. REPORT TYPE AND DATES COVERED
	April 1999	Technical Memorandum

4. TITLE AND SUBTITLE

Implementation and Validation of the Chien k-ϵ Turbulence Model in the Wind Navier-Stokes Code

5. FUNDING NUMBERS

WU-537-05-21-00

6. AUTHOR(S)

Dennis A. Yoder and Nicholas J. Georgiadis

7. PERFORMING ORGANIZATION NAME(S) AND ADDRESS(ES)

National Aeronautics and Space Administration
John H. Glenn Research Center at Lewis Field
Cleveland, Ohio 44135-3191

8. PERFORMING ORGANIZATION REPORT NUMBER

E-11662

9. SPONSORING/MONITORING AGENCY NAME(S) AND ADDRESS(ES)

National Aeronautics and Space Administration
Washington, DC 20546-0001

10. SPONSORING/MONITORING AGENCY REPORT NUMBER

NASA TM—1999-209080
AIAA-99-0745

11. SUPPLEMENTARY NOTES

Prepared for the 37th Aerospace Sciences Meeting & Exhibit sponsored by the American Institute of Aeronautics and Astronautics, Reno, Nevada, January 11-14, 1999. Responsible person, Dennis A. Yoder, organization code 5860, (216) 433-8716.

12a. DISTRIBUTION/AVAILABILITY STATEMENT

Unclassified - Unlimited
Subject Categories: 34, 02, and 61 Distribution: Nonstandard

This publication is available from the NASA Center for AeroSpace Information, (301) 621-0390.

12b. DISTRIBUTION CODE

13. ABSTRACT ***(Maximum 200 words)***

The two equation k-ϵ turbulence model of Chien has been implemented in the WIND Navier-Stokes flow solver. Details of the numerical solution algorithm, initialization procedure, and stability enhancements are described. Results obtained with this version of the model are compared with those from the Chien k-ϵ model in the NPARC Navier-Stokes code and from the WIND SST model for three validation cases: the incompressible flow over a smooth flat plate, the incompressible flow over a backward facing step, and the shock-induced flow separation inside a transonic diffuser. The k-ϵ model results indicate that the WIND model functions very similarly to that in NPARC, though the WIND code appears to be slightly more accurate in the treatment of the near-wall region. Comparisons of the k-ϵ model results with those from the SST model were less definitive, as each model exhibited strengths and weaknesses for each particular case.

14. SUBJECT TERMS	15. NUMBER OF PAGES
Turbulence models; Turbulent boundary layer	25
	16. PRICE CODE: A03

17. SECURITY CLASSIFICATION OF REPORT	18. SECURITY CLASSIFICATION OF THIS PAGE	19. SECURITY CLASSIFICATION OF ABSTRACT	20. LIMITATION OF ABSTRACT
Unclassified	Unclassified	Unclassified	